# Bow shocks in ablated plasma streams for nested wire array z-pinches: A laboratory astrophysics testbed for radiatively cooled shocks[a)]

D. J. Ampleford,[1,b)] C. A. Jennings,[1] G. N. Hall,[2] S. V. Lebedev,[2] S. N. Bland,[2] S. C. Bott,[3] F. Suzuki-Vidal,[2] J. B. A. Palmer,[2] J. P. Chittenden,[2] M. E. Cuneo,[1] A. Frank,[4] E. G. Blackman,[4] and A. Ciardi[5]

[1]*Sandia National Laboratories, Albuquerque, New Mexico 87185-1106, USA*
[2]*The Blackett Laboratory, Imperial College, London SW7 2BW, United Kingdom*
[3]*Center for Energy Research, University of California, San Diego, La Jolla, California 92093, USA*
[4]*Department of Physics and Astronomy, University of Rochester, Rochester, New York 14627, USA and Laboratory for Laser Energetics, University of Rochester, Rochester, New York 14627, USA*
[5]*LERMA, Universite Pierre et Marie Curie, Observatoire de Paris, 5 Place Jules Janssen, Meudon 92195, France*

(Received 1 December 2009; accepted 4 February 2010; published online 4 May 2010)

Astrophysical observations have demonstrated many examples of bow shocks, for example, the head of protostellar jets or supernova remnants passing through the interstellar medium or between discrete clumps in jets. For such systems where supersonic and super-Alfvénic flows and radiative cooling are all important, carefully scaled laboratory experiments can add insight into the physical processes involved. The early stage of a wire array z-pinch implosion consists of the steady ablation of material from fine metallic wires. Ablated material is accelerated toward the array axis by the $J \times B$ force. This flow is highly supersonic ($M > 5$) and becomes super-Alfvénic ($M_A > 2$). Radiative cooling is significant in this flow and can be controlled by varying the material in the ablated plasma. The introduction of wires as obstructions in this steady flow leads to the formation of bow shocks, which can be used as a laboratory testbed for astrophysical bow shocks. The magnetic field associated with this obstruction wire can be controlled by varying the current through it. Differences in the shock for different cooling rates and different magnetic fields associated with the obstruction will be discussed, along with comparisons of dimensionless parameters in the experiments to astrophysical systems. © *2010 American Institute of Physics*. [doi:10.1063/1.3335497]

## I. INTRODUCTION

Supersonic and super-Alfvénic flows are ubiquitous in astrophysics, from material ejected by supernovae to jets produced by young stars and even the solar wind. Many obstructions to these flows exist, for example, as a stellar jet punches through the interstellar medium, or if a static object is present in a wider flow such as the presence of the Earth in the solar wind. Given an appropriate reference frame, these situations are all equivalent to a static object being introduced into a supersonic and/or super-Alfvénic flow.

Taking as an example the bow shock at the head of a protostellar jet, the flow into this shock is supersonic (Mach number $M = v_{\text{flow}}/c_s \sim 10$) and super-Alfvénic (Alfvén Mach number $M_A = v_{\text{flow}}/v_a \sim 4$). Radiative cooling plays a significant role in energy loss in the shock (characterized by a cooling parameter $\chi \sim 1$, which is the ratio of the characteristic cooling time to the characteristic hydrodynamic time scale of the system). The flows into the shock and the structures within the shock are thought to be highly collisional. Depending on the distance from the source star, the plasma $\beta$ (ratio of thermal pressure to magnetic pressure) is typically $\beta \sim 20$.

Laboratory experiments can be used to study this type of system; however there are many challenges in introducing the correct physical processes. Typically on the length scale of the obstruction the flow should be uniform. Radiative cooling plays a critical role in the energy balance of many of these shocks, so should similarly play an important role in the laboratory experiments. Finally such bow shocks are often dominated by the magnetic field pressure due to either a magnetic field associated with the obstruction or an embedded field in the flow. These magnetic field effects can be summarized by two dimensionless parameters, the plasma $\beta$ which describes the importance of magnetic pressure on the dynamics, and the magnetic Reynolds number ($R_m$), which characterizes the importance of Ohmic dissipation.

In this paper we describe a laboratory testbed for the study of radiatively cooled shocks and potentially for the study of magnetically dominated shocks. Experiments utilize the MAGPIE pulsed power generator (1 MA, 250 ns). A modification of the wire array z-pinch[1] is used in which cylindrically convergent supersonic, super-Alfvénic flows interact with a second concentric set of wires which act as obstructions to the flow. This configuration is referred to as a nested wire array (Fig. 1) and is described in detail in Sec. II. Data from the experiments are discussed in Sec. III, Sec. IV discusses simulations of this system, and we conclude in Sec. V by making comparisons of the experiments to specific astrophysical phenomena and by suggesting further modifications to the experiments.

[a)]Paper UI3 5, Bull. Am. Phys. Soc. **54**, 301 (2009).
[b)]Invited speaker. Electronic mail: damplef@sandia.gov.

 © 2010 American Institute of Physics

Downloaded 18 Jan 2011 to 134.253.26.11. Redistribution subject to AIP license or copyright; see http://pop.aip.org/about/rights_and_permissions

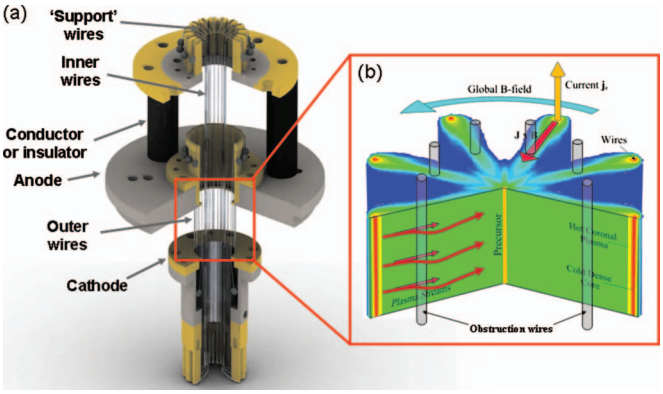


FIG. 1. (Color) (a) Hardware for the nested wire array. The inner wires are suspended by a *spider web* of wires at the top and bottom of the assembly, which allows for good diagnostic access upstream and downstream of the shocks. (b) MHD simulations showing density distribution of ablation streams from the outer wires. Inner wires are superimposed on the flow to illustrate their relative location.

## II. SETUP FOR PRODUCING SHOCKS IN SUPER-ALFVÉNIC FLOWS WITH WIRE ARRAY z-PINCHES

Wire array z-pinches consist of a number of fine metallic wires positioned symmetrically around a common axis, typically in a cylindrical arrangement. A fast rising current leads to ablation of these wires.[2] After initial resistive heating of the wires occurs, a corona forms around the dense wire cores. Plasma streams are accelerated from this corona toward the array axis by the $J \times B$ force.[2] This steady flow of ablated material toward the axis exists for a significant fraction of the experiment ($\sim 200$ ns for a 250 ns current pulse). The flows are supersonic and after the initial acceleration region, these are super-Alfvénic.[3] Experimental data have been used to determine that the velocity of ablated material is relatively fixed in time, typically 15 cm/$\mu$s. The density of the flow increases with current through the wire array and the mass ablation rate can be approximated as proportional to the square of the current through the array.[2] Depending on the initial mass of the array and the magnitude of the current drive, eventually the wires in the array can run out of mass. The majority of the material is then accelerated to the array axis, producing an x-ray burst as it stagnates.

In this paper we are concerned with the ablation flows prior to the array implosion. It is relatively simple to position an obstruction within the convergent flow from the outer wires, such as placing a second set of wires concentric to the first. This setup is in fact frequently used for applications of wire arrays, such as a radiation source for inertial confinement fusion[4,5] and as a K-shell radiation source.[6]

Experiments are performed on the MAGPIE pulsed power generator,[7] which provides a 1 MA current pulse with a rise time of $\sim 250$ ns. The experimental setup for these experiments is shown in Fig. 1. Two concentric (nested) arrays were used. The outer array contained 32 Aluminum wires, each with a 10 $\mu$m diameter, and the inner array consisted of 16 Aluminum wires, each with a 15 $\mu$m diameter. Experiments aim to have the option of interacting the flow with a purely hydrodynamic obstruction. The inner array was longer than the outer to minimize the current through the inner array (as discussed in Refs. 4 and 8), and hence control the magnetic field associated with this obstruction. The level of current through this inner array has previously been determined analytically and experimentally to be 2%–3% of the total machine current, and it can be varied by adjusting the length of the inner array or changing the material used to connect it to the pulsed power driver.[4]

With the addition of obstructions in the ablation flow of the wire array, we expect the formation of shocks. The flow upstream of the shock is characterized by typical parameters observed in wire array experiments. An analytical rocket model[2] provides a good description of the radial mass distribution using the flow velocity measured on MAGPIE of $v_{\text{flow}} \sim 1.5 \times 10^7$ cm/s. At the location of the inner wire array, the mass density in the streams is estimated at $\rho \sim 3 \times 10^{-5}$ g/cm$^3$, which for aluminum gives an ion density of $6.7 \times 10^{17}$ cm$^{-3}$. Given a typical temperature of 10 eV (Ref. 2) and using a Thomas–Fermi average atom model to recover an average ionization of 5, the ion-ion mean free path due to the thermal velocity in the flow is $\sim 0.01$ $\mu$m.

If we first consider just the thermal pressure around an inner wire, the downstream flow parameters can be approximated with the assumption of a planar strong shock using the standard Rankine–Hugoniot jump conditions.[9] Assuming $\gamma = 5/3$, the density jump across the shock is 4 with an associated decrease in the flow velocity (this jump will be reduced if the shock is oblique rather than planar). Given the high Mach number of the upstream flow, the upper limit to the downstream velocity is the local sound speed. The fourfold density increase along with an increase in the ion temperature to $\sim 110$ eV and of mean ionization state to $Z \sim 12$ (neglecting losses to radiation) gives $c_s \sim 9 \times 10^6$ cm/s.

The strong dependence of the ion-ion mean free path on the velocity ($\propto v_{\text{ion}}^4$) greatly reduces the mean free path as the flow becomes subsonic and values are $<0.01$ $\mu$m. These estimates suggest that the flow is collisional upstream of the shock, and the subsequent decrease in the mean free path indicates that the upstream conditions for any secondary shocks would similarly be collisional. A quantitative example of the flow parameters across the shock is taken from simulations and described in Sec. IV.

In addition to being supersonic, the flow from the outer array is also super-Alfvénic. Previous simulation work has estimated Alfvén Mach numbers $\sim 2-3$ midway between the wires and the axis in a single wire array (equivalent to the inner array location in a nested wire array).[10] These simulations also indicate a magnetic Reynolds number $\sim 10$,[10] hence diffusion is relatively unimportant. Assuming just the flow from the outer wire array, the magnetic field pressure at the inner array location is small compared to the ram pressure in the flow. The addition of a current through the inner array will perturb the magnetic field profile, giving an additional local magnetic field around each inner wire. To estimate where the shock may occur in this case, we can calculate the location at which the ram pressure of the flow and the magnetic pressure due to the inner array current are balanced. Using the density and velocity values given

Downloaded 18 Jan 2011 to 134.253.26.11. Redistribution subject to AIP license or copyright; see http://pop.aip.org/about/rights_and_permissions

previously, the ram pressure ($\rho v_{\text{flow}}^2$) equals the magnetic pressure when the local field is $B \sim 40$ T. Given that the current in each inner wire is 1.2 kA this balance occurs at a radius of 6 $\mu$m, which is comparable to the inner wire radius. It is therefore feasible that the shock structure is dominated by the magnetic field due to the inner wire current.

A similar setup previously fielded in Refs. 4 and 8 was modified for this work such that the inner wires are suspended by a spider-web-like mesh of thicker wires. This allows access to the precursor streams both before and after they pass the inner wires for diagnostics positioned end-on to the array (looking down the axis of symmetry of the wire array). The primary diagnostic for these experiments was a time-resolved pinhole camera system looking down the axis (*end-on* to the array) recording images in the extreme-UV (XUV) [$h\nu > 20$ eV (Ref. 11)]. This instrument provides four frames, each with temporal resolution of 2 ns and spatial resolution of 180 $\mu$m.

## III. EXPERIMENTAL DATA

We start by considering the formation of shocks in this setup when there is a small magnetic field associated with the inner array (the standard current division for nested wire array z-pinches). Figure 2 shows an end-on XUV image of one-quarter of the array.

In the image the plasma flow from the outer array is traveling from the top left to bottom right (purple arrows). Inner wires (one indicated in blue) are backlit by the flow, hence are lighter than the emitting (dark) flow around them. As the flows pass the inner wire multiple bow shocks are formed. These appear as an arc around each inner wire which, further from the wire, become straight shocks which are oblique to the flow (red lines). Where these bow shocks meet secondary shocks are formed. These secondary shocks are likely the collision of material that was redirected in the primary shocks. The view in Fig. 2(a) is complicated by the fact that the diagnostic is not viewing directly along the inner wire and surface of the shock, and instead there are some perspective effects [see Fig. 2(b)].

For the discussion here we will assume that the inward plasma flow upstream of the shock is uniform. Figure 2 shows that there is some variation in emission, and hence in either density or temperature. While these are likely to influence the details of the shock, the global structures are unlikely to be significantly affected. This is demonstrated experimentally in the figure by the shocks being symmetric around each inner wire, despite the discrete flows into the shock not being azimuthally uniform.

The imaging system used to diagnose the array takes multiple images of the array (at different azimuthal locations and times), hence we can determine whether this shock angle changes in time. Figure 3 shows the shock in the experiment shown in Fig. 2 at three additional times (these are at different azimuthal locations). Significantly, there is very little variation in the shock angle with time in these images. This fixed structure and angle in time are expected given the slow variation in the mass ablation rate (with characteristic time of $\sim 200$ ns) in comparison with the characteristic time scale for the flow to cross the shock ($\sim 1$ ns). Hence on the characteristic time scale of the shock the system is quasistatic.

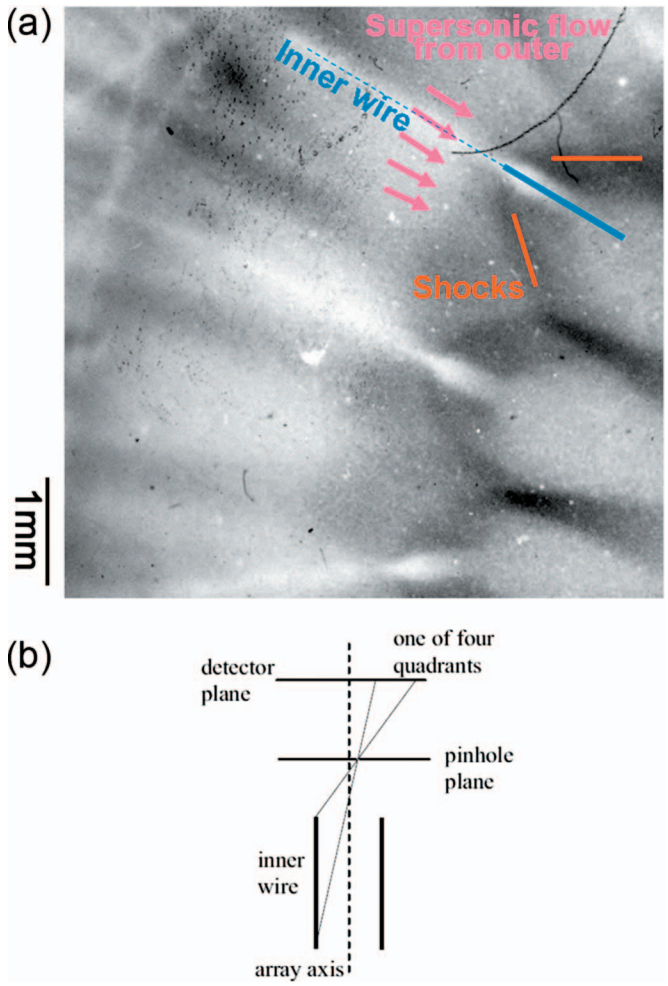


FIG. 2. (Color) XUV imaging of the system looking down the axis 232 ns after the start of current. This image shows one quadrant of the system. In this and later figures, dark represents emission and light represents nonemitting regions. The flow from the outer arrays is convergent toward the axis, which is at the bottom right of the image. The data show the formation of shocks (dark curved structures) around each of the inner wires (lighter stripes which are due to perspective appear to be diverging from the center of the image; the wires are backlit by the shocks). (b) shows an illustration of the perspective effects of this diagnostic.

In Fig. 2 the half opening angle of the shock (the angle of the shock to the original flow trajectory) is measured to be

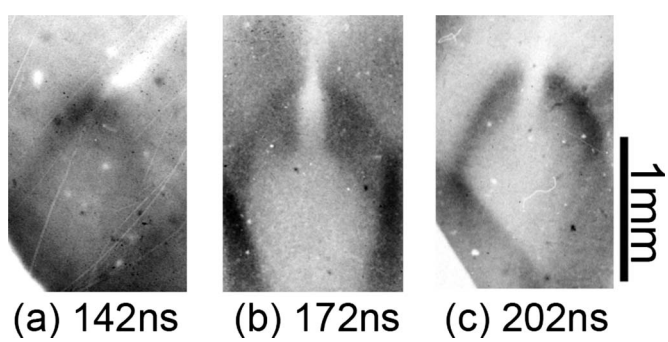


FIG. 3. Small segments of the array at three different times (due to the diagnostic setup these are at different azimuthal locations). The shock shape appears static in time. The image intensities have been adjusted to demonstrate the shock features at each time.

Downloaded 18 Jan 2011 to 134.253.26.11. Redistribution subject to AIP license or copyright; see http://pop.aip.org/about/rights_and_permissions

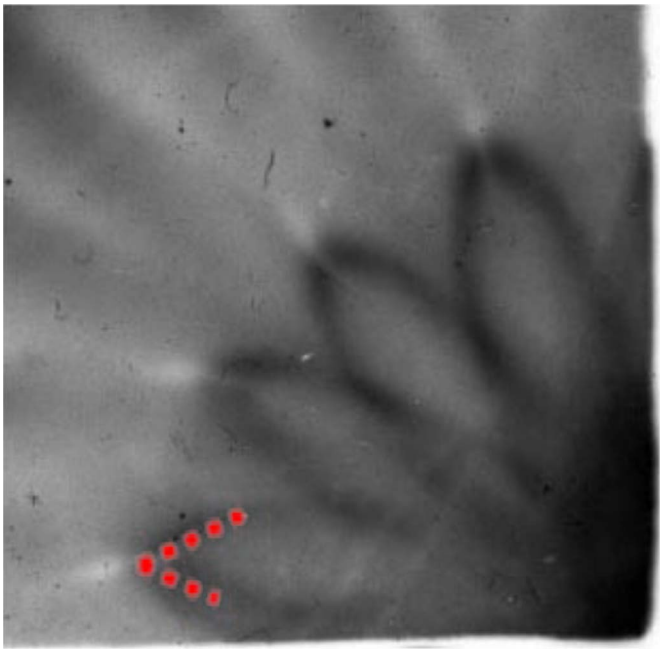

FIG. 4. (Color online) An XUV image equivalent to Fig. 2, except the inner array is isolated from the pulsed power drive voltage, and hence has less field associated with it than the previous case. As in Fig. 2, the incoming flow is Al.

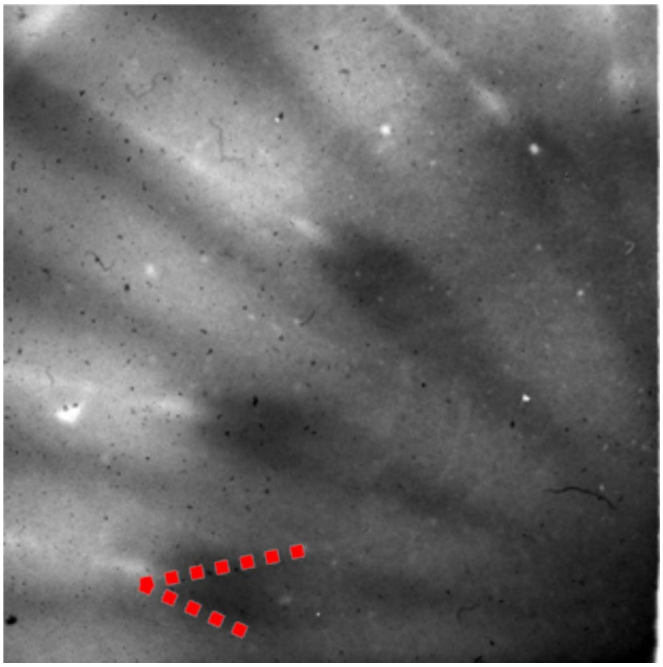

FIG. 5. (Color online) End on image of a tungsten wire array, showing dramatically smaller shock opening angle [this image is at 184 ns after the start of current, at a similar time to Fig. 3(b)]. The electrode configuration is similar to Fig. 2, allowing some current through the inner wire array.

≈40°. The structure of the shock, and more specifically the opening angle and shape, are likely to be impacted by the size of the obstruction. Previous radiography of the inner wires in a similar experimental setup on MAGPIE has shown that the physical size of the dense wire cores is ~20 $\mu$m. This is larger than the initial inner wire diameter, but notably is smaller than the scale length of the shock (e.g., the shock thickness in Fig. 2 ~100–200 $\mu$m), hence the shock is likely to be attached to the obstruction,[12] and will not be a strong function of the obstruction size. Additionally, the experimental setup used in Fig. 2 allows some of the machine current to pass through the inner wires. It is likely that the magnetic field pressure created by this current has an effect on the shock geometry.

The system used in Fig. 2 can be adapted to reduce the current associated with the inner wires. With the electrode setup shown in Fig. 1 a few percent of the machine current passes through the inner array.[4] By replacing the conducting connection to the inner wires with an insulated (plastic) support, we can eliminate all current associated with this inner array. In this case the wires act as a purely hydrodynamic obstruction to the magnetohydrodynamic (MHD) flow from the outer wires. By reducing the current through the inner array, the field upstream of the obstruction is modified, hence the magnetic pressure and Alfvén velocity will each be reduced (in turn, increasing both the plasma $\beta$ and the Alfvén Mach number in the flow).

Figure 4 shows the data for this case. Comparing Figs. 2 and 4 we see that with less current (and hence field) associated with the inner array the shock half opening angles are reduced from 40° to 20°. Although no direct measures of the plasma parameters before and after the shock are available at present, it is assumed the change is due to the variation in the Alfvén Mach number and the plasma $\beta$.

While the earlier estimates showed that the shock profile may be determined here by the B-field associated with the inner wires, the proximity of the shock to the wire position and the limited resolution of the imaging system means that it is not possible to conclusively rule out the effect of the size of the obstruction, which may be slightly larger when current flows in the inner array. Rather than reducing the current as we have done in Fig. 4, it is simple to modify the experiment to increase the current level in the inner wire to increase the local field strength to more closely examine this. For example, reducing the inner wire array to a single wire would increase the current, and hence B-field, by a factor of 16. The balance of the flow ram pressure and the magnetic pressure at this single obstruction occurs at a radius of ~130 $\mu$m. By radially offsetting the imaging system and increasing the magnification, an ideal line of sight and resolution can be obtained, which could resolve the shock position. Such a modification could form the basis of future studies.

In addition to the effects of the magnetic field, we can test the effects of radiative cooling on the system. For a fixed upstream flow velocity and obstruction configuration, an increase in the rate of radiative cooling will reduce the post-shock temperature, hence leading to a narrower shock opening angle.

For the densities and temperatures of the plasma flows in these experiments, the rate of radiative cooling increases with atomic number,[13] hence we can vary this cooling time scale by varying the material of the wire array (in a similar manner to Ref. 14).

Figure 5 shows the bow shocks formed when a tungsten

Downloaded 18 Jan 2011 to 134.253.26.11. Redistribution subject to AIP license or copyright; see http://pop.aip.org/about/rights_and_permissions

flow meets an obstruction. The data indicate that the shock half opening angle has been significantly reduced from ~40° for the shock in Al flow in Fig. 2 to ~15° for the shock in the W flow in Fig. 5. Further understanding of this system can be gained and more direct connection to astrophysical systems can be made, by comparisons of these experimental data to simulations.

## IV. COMPARISONS TO SIMULATIONS

The GORGON MHD code[15] has been used to simulate these experiments. This is a three-dimensional (3D) resistive MHD code, utilizing an optically thin simple recombination radiation loss model.[15] This code has previously been used to model both wire array z-pinches[3,15] and protostellar jets.[16] To achieve the resolution required to study the shocks found in the experiment in detail, we will discuss two-dimensional (2D) simulations in a plane perpendicular to the array wires. We note that many of the 3D effects that occur in wire array z-pinches normally manifest themselves after wire breakage, which is later than the times of interest in this discussion. It is not possible to model the longer inner array used in the experiments in 2D. The experimental purpose of this longer inner array is to minimize the current through the inner array in experiments with relatively low wire numbers in the outer array. In these simulations of the MAGPIE experiments we instead use unphysically high outer wire numbers to inductively screen the inner array, hence recreating the 2%–3% of current determined for this setup on MAGPIE.

Figure 6 shows the results of an MHD simulation for an Al nested array on MAGPIE at 200 ns. Figure 6(a) shows the density profile within the array. The presence of inner wires leads to the formation of bow shocks around each of the inner wires. The simulated emission [Fig. 6(b)] shows a broadly similar structure to the experimental emission [Fig. 6(d)]. The experimental shock angles are a factor of ~2 larger than is found in the simulation. This discrepancy illustrates the need for this type of experimental result in order to benchmark simulations, both for modeling laboratory experiments and astrophysical modeling. Further work is needed, however the general characteristics are reproduced and we are still able to interrogate the present simulation about some of the important physical processes.

The magnetic field structure within the array is shown in Fig. 6(c). As expected, due to the inductive current division between the inner and outer wires, minimal current flows in the inner array, hence there is only a small perturbation to the field in the vicinity of the inner wires. The magnetic field plot does indicate that there is some perturbation of the field after the flows have passed the inner array. From the plasma parameters given by these calculations, we find that the magnetic Reynolds number $R_m \sim 8$. This value indicates that a relatively small proportion of the field is advected with the flow; however the experiments are unlikely to be in the $R_m \gg 1$ regime typical of many astrophysical systems. This and many of the other MHD quantities derived from the simulation are summarized in Table I.

Figure 7 shows various lineouts of the calculation results, taken between two inner wires [at the location indicated in red on Fig. 6(a)]. The lineout of density [Fig. 7(a)] shows the density jump through the shock, and is matched by a drop in flow velocity [Fig. 7(b)]. The density increases by a factor of ~4, indicating that this is a strong shock. This is expected given the high Mach number and Alfvén Mach number [Fig. 7(c)].

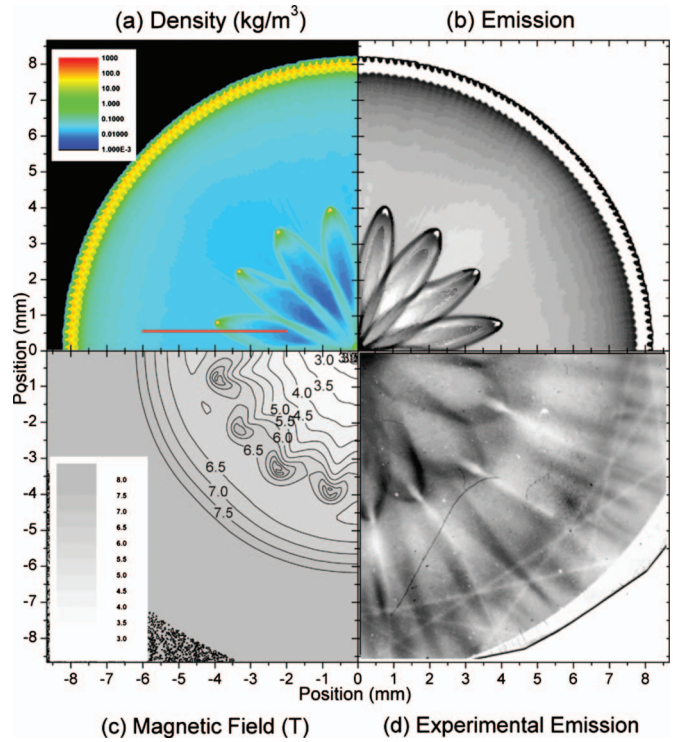


FIG. 6. (Color) The results of MHD simulations of the nested wire array system at 200 ns showing (a) density (kg/m$^3$), (b) simulated emission (dark regions on the image correspond to high emission), and (c) magnetic field strength ($T$). Also shown (d) is self-emission from the experiment for comparison. The red line on (a) denotes the location of the lineout used in Fig. 7

It is notable that the local Mach number postshock is >1. This is possible as the shock is oblique rather than planar, hence the nonperpendicular component of the velocity is not impacted by the shock jump conditions. If the shock was planar, the importance of radiative cooling in this system suggests that the density jump would be >4.[9]

If we calculate the plasma $\beta$ (ratio of plasma pressure to magnetic pressure resulting from both the field advected with the flow and the local field around the obstruction) at this

TABLE I. Dimensionless parameters of solar wind, protostellar bow shock, and bow shock in nested wire array. Parameters for the nested wire array experiments are based on the MHD simulations discussed.

| Parameter | Symbol | Solar wind | Protostellar bow shock | Wire array |
|---|---|---|---|---|
| Mach Number | M | 9 | 10 | 4–12 |
| Alfvén Mach number | $M_A$ | 9 | 4 | 1–5 |
| Plasma beta | $\beta$ | 0.8 | 20 | 0.1–5 |
| Magnetic Reynolds number | $R_m$ | $10^9$ | $10^8$ | 4–10 |
| Localization | mfp/r | 1 | $10^{-6}$ | $10^{-5}$ |

Downloaded 18 Jan 2011 to 134.253.26.11. Redistribution subject to AIP license or copyright; see http://pop.aip.org/about/rights_and_permissions

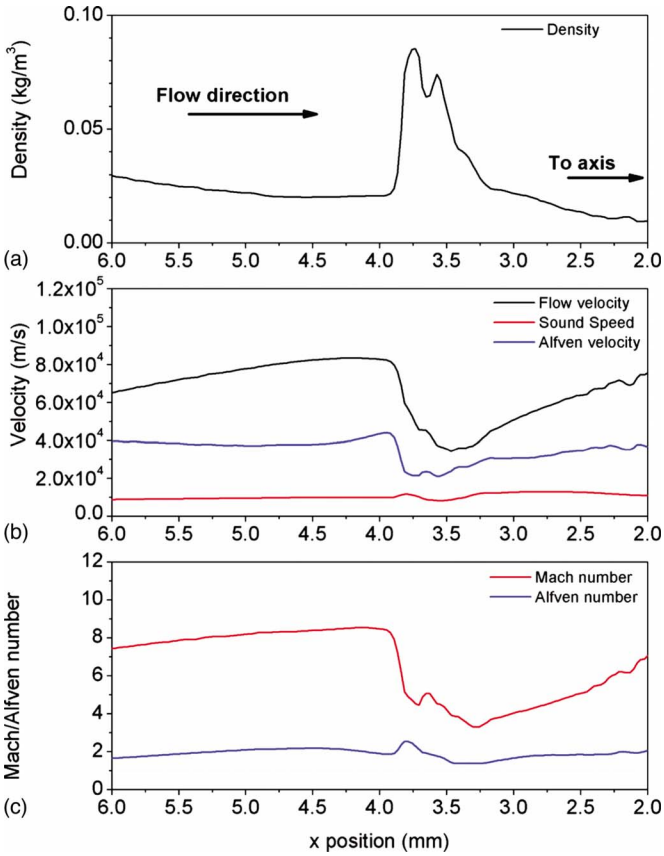


FIG. 7. (Color online) (a) Density profile through the shock showing the jump conditions. (b) Velocity upstream and downstream of the shock, along with local sound speeds and Alfvén velocities. (c) Mach numbers and Alfvén Mach numbers through the shocks. The location of the lineouts is shown in Fig. 6(a).

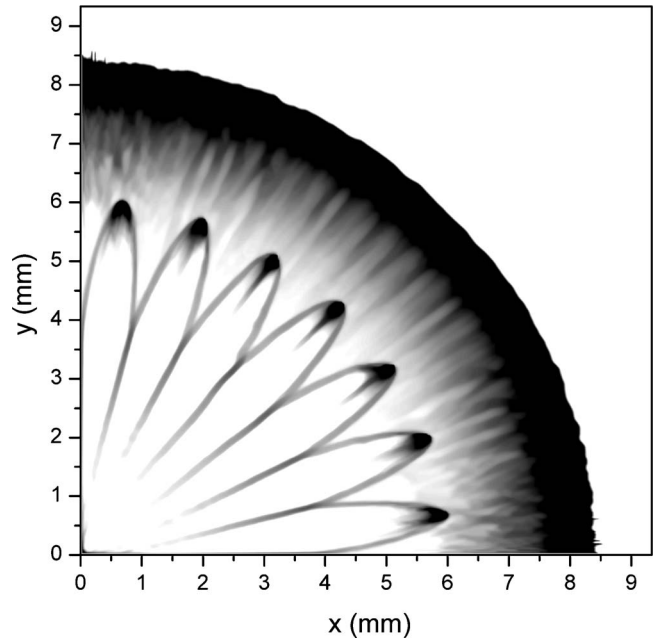


FIG. 8. Simulation emission profile for a nested array on the Z generator. Dark represents emission; light represents nonemitting regions. This image is ~10 ns prior to the interaction pulse for a nested wire array with a 2.5 mg outer array and a 2.5 mg inner array.

location we see that $\beta \sim 0.4$, indicating a significant role of the magnetic field in the pressure balance of the shock, as was demonstrated in the experiment by the change in shock angle with the change in field.

## V. DISCUSSION

Wire array z-pinches have been used to produce bow shocks around a sequence of small obstructions (another wire array). Data indicate that the angles of shocks are static in time, but they are altered by varying the current through the inner array. This is likely due to the change in the local magnetic field surrounding each of the inner wires, although the effect of the difference in the obstruction size cannot be dismissed. If the magnetic field effects are dominant, there are two possible mechanisms for this field to affect the shock structures. First, the MHD simulations indicate that some of the field is frozen into the flow ($R_m > 1$). Consequently the magnetic pressure associated with the field around the inner wires will act to decelerate the flow from the outer array. Alternatively the field from the inner array is altering the magnetic field upstream from the shock, and will alter the Alfvén Mach number before the shock.

Table I shows a comparison of some important dimensionless scaling parameters for this system and two contrasting astrophysical bow shocks: the magnetosphere and the bow shock of a protostellar jet. Significant further work is required to tune these experiments to model specific astrophysical bow shocks.

One of the most contrasting values in the comparison between the three cases is the localization parameter. The solar wind is collisionless, the protostellar jet case is highly collisional, and the array case discussed is between the two. Given that the mean free path is dependent on the plasma density, the dependence of density on machine current can be utilized to provide control over the localization. To increase the density and hence reduce the mean free path, experiments can be performed at higher currents. Figure 8 shows that very similar shocks are formed for nested arrays on the Z generator (20 MA, 100 ns) at Sandia National Laboratories. This nested array configuration is routinely fielded on Z,[5,6] hence much insight could be gained by diagnosing these shocks around the inner array wires (the shock structures discussed in this paper may have a significant effect on radiation pulse shaping with nested wire arrays, which will be discussed fully in a future paper).

In the other direction, reducing the current and increasing the array diameter would shift more into a collisionless regime. Such experiments are planned on the 250 kA, 150 ns GenASIS machine at University of California, San Diego.[17] Controls of the dimensionless parameters in Table I can also be gained by modifying the array setup, and simple changes can optimize the experimental parameters for specific regimes.

The plasma $\beta$ in the current experiments is lower than those found in the astrophysical systems (Table I). It is possible to impose an axial magnetic field in the incoming flow by twisting the outer array,[18] which will have the effect of increasing the magnetic pressure within the flow. The Alfvén

Downloaded 18 Jan 2011 to 134.253.26.11. Redistribution subject to AIP license or copyright; see http://pop.aip.org/about/rights_and_permissions

Mach number of the flow can be varied by moving the inner wire; locating the inner wire at ~6–7 mm would mean that the shock is at the trans-Alfvénic point in the flow, allowing experiments to study shocks in the regime $M_A \sim 1$ (for W this point would be at ~5 mm).

Other improvements to this type of experiments could be to modify the array configuration such that the flow is less cylindrically convergent, for example, attempting to modify the linear wire array setup discussed in Ref. 19. Alternatively, to investigate shocks in divergent rather than convergent geometry an exploder inverse-z-pinch could be fielded,[20] with the flow moving outward from the source array to the obstruction wires. A further extrapolation of the discussed experiment would be to investigate the effect of obstruction size on the shocks created.[12]

In addition to modifications to the wire array configuration, in future work it would be critical to obtain more quantitative data from the experiments. This could include end-on interferometry[21] or radiography[22] to obtain density measurements (particularly important for diagnosing shock jump conditions), spatially and temporally resolved spectroscopy to determine local electron temperature[23] and Faraday rotation or B-dot probes to diagnose the magnetic field structure.

In summary, these experiments have established an interesting laboratory testbed for radiatively cooled bow shocks. Control over cooling and magnetic field pressures has been demonstrated, and simulations have recovered many of the structures observed. Future work will aim to optimize these experiments to specific astrophysical scenarios.

## ACKNOWLEDGMENTS

Sandia is a multiprogram laboratory operated by Sandia Corporation, a Lockheed Martin Co., for the United States Department of Energy's National Nuclear Security Administration under Contract No. DE-AC04-94AL85000. This work was in part supported by the SSAA program of the NNSA under DOE Cooperative Agreement No. DE-FC03-02NA00057.

[1] M. K. Matzen, M. A. Sweeney, R. G. Adams, J. R. Asay, J. E. Bailey, G. R. Bennett, D. E. Bliss, D. D. Bloomquist, T. A. Brunner, R. B. Campbell, G. A. Chandler, C. A. Coverdale, M. E. Cuneo, J.-P. Davis, C. Deeney, M. P. Desjarlais, G. L. Donovan, C. J. Garasi, T. A. Haill, C. A. Hall, D. L. Hanson, M. J. Hurst, B. Jones, M. D. Knudson, R. J. Leeper, R. W. Lemke, M. G. Mazarakis, D. H. McDaniel, T. A. Mehlhorn, T. J. Nash, C. L. Olson, J. L. Porter, P. K. Rambo, S. E. Rosenthal, G. A. Rochau, L. E. Ruggles, C. L. Ruiz, T. W. L. Sanford, J. F. Seamen, D. B. Sinars, S. A. Slutz, I. C. Smith, K. W. Struve, W. A. Stygar, R. A. Vesey, E. A. Weinbrecht, D. F. Wenger, and E. P. Yu, Phys. Plasmas **12**, 055503 (2005).
[2] S. V. Lebedev, F. N. Beg, S. N. Bland, J. P. Chittenden, A. E. Dangor, and M. G. Haines, Phys. Plasmas **9**, 2293 (2002).
[3] J. P. Chittenden, S. V. Lebedev, S. N. Bland, A. Ciardi, and M. G. Haines, Phys. Plasmas **8**, 675 (2001).
[4] S. N. Bland, S. V. Lebedev, J. P. Chittenden, C. Jennings, and M. G. Haines, Phys. Plasmas **10**, 1100 (2003).
[5] M. E. Cuneo, D. B. Sinars, E. M. Waisman, D. E. Bliss, W. A. Stygar, R. A. Vesey, R. W. Lemke, I. C. Smith, P. K. Rambo, J. L. Porter, G. A. Chandler, T. J. Nash, M. G. Mazarakis, R. G. Adams, E. P. Yu, K. W. Struve, T. A. Mehlhorn, S. V. Lebedev, J. P. Chittenden, and C. A. Jennings, Phys. Plasmas **13**, 056318 (2006).
[6] C. A. Coverdale, C. Deeney, B. Jones, J. Thornhill, K. G. Whitney, A. L. Velikovich, R. W. Clark, Y. K. Chong, J. P. Apruzese, J. Davis, and P. D. LePell, IEEE Trans. Plasma Sci. **35**, 582 (2007).
[7] I. H. Mitchell, J. M. Bayley, J. P. Chittenden, J. F. Worley, A. E. Dangor, M. G. Haines, and P. Choi, Rev. Sci. Instrum. **67**, 1533 (1996).
[8] S. V. Lebedev, R. Aliaga-Rossel, S. N. Bland, J. P. Chittenden, A. E. Dangor, M. G. Haines, and M. Zakaullah, Phys. Rev. Lett. **84**, 1708 (2000).
[9] Y. B. Zel'dovich and Y. P. Raizer, *Physics of Shock Waves and High-Temperature Hydrodynamic Phenomena* (Academic, New York, 1967).
[10] J. P. Chittenden, S. V. Lebedev, B. V. Oliver, E. P. Yu, and M. E. Cuneo, Phys. Plasmas **11**, 1118 (2004).
[11] S. N. Bland, D. J. Ampleford, S. C. Bott, S. V. Lebedev, J. B. A. Palmer, S. A. Pikuz, and T. A. Shelkovenko, Rev. Sci. Instrum. **75**, 3941 (2004).
[12] J. D. Anderson, *Modern Compressible Flow with Historical Perspective*, 2nd ed. (McGraw-Hill, New York, 1990).
[13] D. E. Post, R. V. Jensen, C. B. Tarter, W. H. Grasberger, and W. A. Lokke, At. Data Nucl. Data Tables **20**, 397 (1977).
[14] S. V. Lebedev, J. P. Chittenden, F. N. Beg, S. N. Bland, A. Ciardi, D. Ampleford, S. Hughes, M. G. Haines, A. Frank, E. G. Blackman, and T. Gardiner, Astrophys. J. **564**, 113 (2002).
[15] J. P. Chittenden, S. V. Lebedev, C. A. Jennings, S. N. Bland, and A. Ciardi, Plasma Phys. Controlled Fusion **46**, B457 (2004).
[16] A. Ciardi, D. J. Ampleford, S. V. Lebedev, and C. Stehle, Astrophys. J. **678**, 968 (2008).
[17] S. C. Bott, D. M. Haas, Y. Eshaq, U. Ueda, R. E. Madden, G. W. Collins IV, and F. N. Beg, "Ablation Studies of Low-Number Wire Arrays at 200 kA Using a Linear Transformer Driver," IEEE Trans. Plasma Sci. (to be published).
[18] S. C. Bott, S. V. Lebedev, D. J. Ampleford, S. N. Bland, J. P. Chittenden, A. Ciardi, M. G. Haines, C. Jennings, M. Sherlock, G. Hall, J. Rapley, F. N. Beg, and J. Palmer, Phys. Rev. E **74**, 046403 (2006).
[19] S. N. Bland, S. V. Lebedev, J. P. Chittenden, D. J. Ampleford, and G. Tang, Phys. Plasmas **11**, 4911 (2004).
[20] A. J. Harvey-Thompson, S. V. Lebedev, S. N. Bland, J. P. Chittenden, G. N. Hall, A. Marocchino, F. Suzuki-Vidal, S. C. Bott, J. B. A. Palmer, and C. Ning, Phys. Plasmas **16**, 022701 (2009).
[21] S. V. Lebedev, F. N. Beg, S. N. Bland, J. P. Chittenden, A. E. Dangor, M. G. Haines, K. H. Kwek, S. A. Pikuz, and T. A. Shelkovenko, Phys. Plasmas **8**, 3734 (2001).
[22] I. C. Blesener, J. B. Greenly, S. A. Pikuz, T. A. Shelkovenko, S. Vishniakou, D. A. Hammer, and B. R. Kusse, Rev. Sci. Instrum. **80**, 123505 (2009).
[23] P. W. Lake, J. E. Bailey, G. A. Rochau, T. C. Moore, D. Petmecky, and P. Gard, Rev. Sci. Instrum. **75**, 3690 (2004).

Downloaded 18 Jan 2011 to 134.253.26.11. Redistribution subject to AIP license or copyright; see http://pop.aip.org/about/rights_and_permissions